Theoretical determination of two-electron one-photon transition characteristics for low-Z K-shell hollow atoms

Karol Kozioł[*] and Jacek Rzadkiewicz[†]

Narodowe Centrum Badań Jądrowych (NCBJ), Andrzeja Sołtana 7, 05-400 Otwock-Świerk, Poland

(Received 22 June 2017; published 14 September 2017)

Studying K-shell hollow atom spectra broadens our knowledge on femtosecond phenomena in atomic physics, chemistry, and biology. Recent synchrotron measurements of the two-electron one-photon (TEOP) transitions of low-Z atoms have shown discrepancies between experiment and theoretical predictions of the TEOP relative intensities and their linewidths. The discrepancies seem to be a result of an incomplete description of an atomic response to the strong perturbation due to the K-shell double photoionization (DPI). A theoretical attempt, based on the multiconfiguration Dirac-Fock relativistic configuration interaction method, is presented for Mg, Al, and Si atoms. It is demonstrated that both the branching ratios and the TEOP linewidths can be closely reproduced by taking into account the influences of the core and valence electron correlations, open-shell valence configuration, and the outer-shell ionization and excitation processes following the K-shell DPI.

K-shell hollow atoms, i.e., atoms in which electrons fill the outer shells while the innermost shell is entirely empty, constitute an attractive environment for studies of the nature of exotic atomic states and of mechanisms leading to their production. Such atoms can be produced in many physical processes, including nuclear decays and ion-atom collisions. K-shell hollow atoms can also be produced by the K-shell absorption of a single photon followed by a purely quantum mechanical shake-off or by a (quasi)classical knockout process [1–3]. Another mechanism responsible for producing K-shell hollow atoms is a sequential multiphoton absorption on a time scale comparable with its decay time [4,5]. The latter requires very short, intense x-ray pulses induced, e.g., by a free electron laser [6,7].

K-shell hollow atoms decay by nonradiative Auger or radiative transitions. The radiative transitions can occur via one-electron one-photon (OEOP) or via much less probable two-electron one-photon (TEOP) transitions (see Fig. 1). The OEOP process in which an electron jumps from the $2p$ subshell to the empty K shell ($1s^{-2} \rightarrow 1s^{-1}2p^{-1}$) is accompanied by a single x-ray photon emission. In the case of the TEOP process, the empty K shell is completely filled by simultaneous transitions of two electrons from the L shell ($1s^{-2} \rightarrow 2s^{-1}2p^{-1}$) also with the emission of a single x-ray photon. Both OEOP and TEOP transitions are very sensitive to the Breit interaction, quantum electrodynamics (QED), and electron correlations [8–10]. Moreover, the natural widths of the corresponding $K^h\alpha$ and $K\alpha^h$ lines give direct information on the K-shell hollow atoms lifetimes, which are the shortest lifetimes of any known bound atomic state [3,11–13]. Thus, the TEOP and OEOP transitions permit exploring both the fundamentals of atomic physics and the nature of the K-shell double photoionization (DPI) processes.

The TEOP transitions were predicted for the first time by Heisenberg [14] in 1925. In 1931 Goudsmit and Gropper [15] formulated the corresponding selection rules (i.e., Δn_1, Δn_2 can change arbitrarily, while $\Delta l_1 = \pm 1$, $\Delta l_2 = 0, \pm 2$). In 1975 Wölfli *et al.* reported the first experimental observation of TEOP transitions in Fe and Ni atoms [16]. Since then, the TEOP transitions in K-shell hollow atoms have been investigated in many experiments [17–24].

Recently, the TEOP transitions following single-photon K-shell DPI have been observed in a highly accurate synchrotron experiment for Mg, Al, and Si by Hoszowska *et al.* [3]. In the experiment, the TEOP transition energies, branching ratios of the OEOP to TEOP transitions, and the TEOP linewidths were precisely measured. So far, this single-photon impact data provides the most reliable experimental results, which can rigorously test the most advanced atomic modeling.

A comparison of the experimental values and theoretical predictions has shown a good agreement only for the TEOP energies. The experimental branching ratios of the OEOP to TEOP transitions and the TEOP linewidths are rather poorly reproduced by theory. The calculations based on second-order perturbation theory using single-electron screened hydrogenic wave functions [25] as well as the Hartree-Fock calculations based on a so-called "shake-down" model [26] and the multiconfiguration Dirac-Fock (MCDF) [27] method underestimate the experimental branching ratios [3] by a factor of 2 to 3. It is only the employment of the relativistic configuration interaction (RCI) formalism that allows reducing the discrepancies to the level of 15%–30% [10]. In the case of TEOP linewidths, it was found that the measured values are larger by a factor of $\sim$2 (or $\sim$1.6 with the Γ_{KK} correction) than the theoretical estimates based on the sum of the initial and final state widths (for details, see [3]). Therefore, it is clear that accurate calculations of the TEOP intensities for low-Z elements are called for [28].

In this work, we report a comprehensive theoretical attempt to reproduce the $K\alpha\alpha^h$ linewidths and branching ratios of the OEOP to TEOP transitions for Mg, Al, and Si measured in Ref. [3]. The fully relativistic calculations of KK atomic level widths and of $L_1L_{2,3}$ widths are also presented.

The calculations of the radiative transition energies and rates were carried out by means of the GRASP2K v1.1 [29] code, based on the MCDF method. The methodology of the MCDF calculations performed in the presented research is similar to that published earlier, in many papers (see, e.g., [30,31]).

[*]Karol.Koziol@ncbj.gov.pl
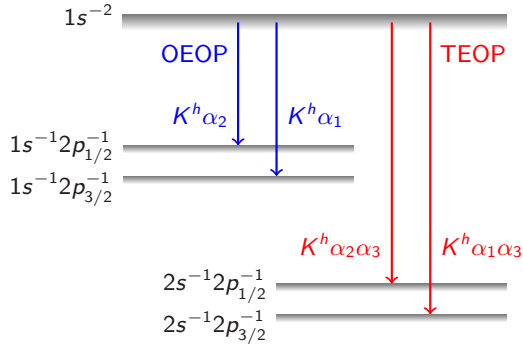
[†]Jacek.Rzadkiewicz@ncbj.gov.pl

FIG. 1. Level scheme (not to scale) showing the decay of K-shell hollow atoms via OEOP (blue arrows) and TEOP transitions (red arrows).

The wave function for an N-electron system is given as an atomic state function (ASF), which is a linear combination of configuration state functions (CSFs). In the calculations, the Breit interaction, self-energy, and vacuum polarization QED corrections have been taken into account [32–34]. The radiative transition rates were calculated in both the velocity (Coulomb) [35] and length (Babushkin) [36] gauges. The accuracy of the wave function depends on the CSFs included in its expansion [37]. The accuracy can be improved by extending the CSF set by including the CSFs originating from substitutions from orbitals occupied in the reference CSFs to unfilled orbitals of the active orbital set [active space (AS)]. The RCI method makes it possible to include a major part of the electron correlation's contribution to the energy of the atomic levels and transition strengths [38,39]. The difference between the transition rates calculated in the length and velocity gauges is a common way to test the quality of a wave function obtained in self-consistent calculations. Kadrekar and

Natarajan found [10] that the discrepancies between the $K\alpha\alpha^h$ transition rates calculated in the length and velocity gauges may be reduced by using the RCI approach. They also found that the transition rates are very sensitive to the choice of the orbital set.

Our studies, performed on a large number of test cases, showed that using substitutions for "hole" orbitals in the RCI expansion is crucial for producing reliable results that take into account important correlation effects. Hence, the $\{ns\}$ ($n = 1$–3) active space was used for the initial states of the $K\alpha\alpha^h$ transitions ($1s^{-2}$) (containing the CSFs produced by $1s$–$2s$ and $1s$–$3s$ substitutions) and the $\{ns,np\}$ ($n = 1$–3) active space was used for the final states ($2s^{-1}2p^{-1}$) (containing CSFs produced by substitutions for "hole" $2s$ and $2p$ orbitals). The RCI expansion was created by using single (S) and double (D) substitutions from a multireference set. In this way the length-velocity transition rate ratio, I_{len}/I_{vel}, may be reduced from 3.58–3.64 to 1.02–1.09. In the next stages, we extended the CSF set to $\{ns,np\}$ ($n = 1 - n_{max}$, $n_{max} = 4,5$) active spaces, excluding only $1s$–$2p$ substitutions for the initial states (because of convergence issues).

In Table I we show the transition rates of the $K\alpha\alpha^h$ transitions for Mg. As one can see in the table, the $K\alpha\alpha^h$ transition rates in length (A^L) and velocity (A^V) forms significantly differ when the virtual orbital contributions are neglected (AS0). Next, using only S substitutions to virtual orbitals does not improve the ratio I_{len}/I_{vel}. In order to get convergence and an agreement between A^L and A^V, one has to extend the calculations to the SD substitutions with an active set at least up to $n = 4$ (AS2). Therefore, to ensure that our calculations take a reasonable time and obtain a reasonable accuracy, we kept the calculations to the AS3 stage for Mg and Al, and the AS2 stage for Si (for which the convergence is more difficult to achieve). The lower part of Table I presents the predictions for the $3s$ satellites of the "pure" TEOP that,

TABLE I. Total transition rates of $K\alpha\alpha^h$ transitions for Mg for various active spaces.

Active space for initial/final states	No. of CSFs[a]		A^L	A^V	A^L/A^V
	$1s^{-2}$	$2s^{-1}2p^{-1}$	(10^{10} s^{-1})		
AS0 $2s^2 2p^6 3s^2/1s^2 2s^1 2p^5 3s^2$	1	2	5.109	1.429	3.575
S substitutions only					
AS1 $\{ns\}/\{ns,np\}$ ($n = 1$–3)	3	20	8.646	2.129	4.062
AS2 $\{ns,np\}$ ($n = 1$–4)[b]	9	48	8.463	2.082	4.064
AS3 $\{ns,np\}$ ($n = 1$–5)[b]	13	76	8.481	2.086	4.065
SD substitutions					
AS1 $\{ns\}/\{ns,np\}$ ($n = 1$–3)	6	200	2.168	1.992	1.088
AS2 $\{ns,np\}$ ($n = 1$–4)[b]	101	954	2.078	1.865	1.114
AS3 $\{ns,np\}$ ($n = 1$–5)[b]	233	2278	2.083	1.862	1.119
Ref. [10] (limited RCI)			0.004	2.574	0.0015
Ref. [10] (large RCI)			2.262	2.169	1.043
Ref. [27]			5.11		
3s satellite (SD substitutions)					
AS0 $2s^2 2p^6 3s^1/1s^2 2s^1 2p^5 3s^1$	1	6	5.871	1.641	3.578
AS1 $\{ns\}/\{ns,np\}$ ($n = 1$–3)	8	493	2.258	2.228	1.014
AS2 $\{ns,np\}$ ($n = 1$–4)[b]	213	2184	2.404	2.220	1.083
AS3 $\{ns,np\}$ ($n = 1$–5)[b]	500	5094	2.459	2.216	1.109

[a]States involved in $K\alpha\alpha^h$ transitions only.

[b]Excluding $1s$–$2p$ substitutions for initial states because of convergence issues.

TABLE II. Total transition rates of $K\alpha\alpha^h$ transitions (in 10^{10} s^{-1}) per $1s^{-2}$ state.

		Present		Ref. [10]			
		A^L	A^V	A^L	A^V	Ref. [40]	Ref. [27]
Mg	diag.	2.083	1.862	2.262	2.169		5.11
	3s sat.	2.459	2.216				
Al	diag.	2.535	2.382	3.248	2.854	9.69	6.61
	3s sat.	3.033	2.689				
	3p sat.	3.029	2.463				
Si	diag.	2.989	2.780	3.407	3.367		8.37
	3s sat.	3.840	3.199				
	3p sat.	3.503	3.047				

due to the outer-shell ionization and excitation (OIE [12]) processes, can noticeably modify the effective (observed in an experiment) transition rates and the corresponding TEOP linewidths, as in the case of OEOP transitions [12]. Similar calculations have been performed for OEOP transitions in Mg and for OEOP and TEOP transitions for Al and Si atoms.

The final values of the transition strengths are presented in Table II together with other theoretical predictions obtained by means of the relativistic MCDF [27,40] and the MCDF-RCI formalism [10], respectively. A good agreement between A^L and A^V indicates the quality of the ASF representations [41]. One can also see that the transition rates for the $3s$ and $3p$ satellites of the $K\alpha\alpha^h$ transitions are about 20%–30% higher than those for the diagram ones. It was also found that in the case of the $3s$ and $3p$ satellites of OEOP ($K^h\alpha$) transitions, the change in the corresponding transition rates is significantly lower (up to 1%). Thus, it is clear that $3s$ and $3p$ OIE processes can modify the branching ratios.

The $K^h\alpha$ and $K\alpha\alpha^h$ branching ratios were calculated by using the expression

$$BR = \frac{I(K^h\alpha)}{I(K\alpha\alpha^h)} = \frac{\sum_{ij} A_{ij}}{\sum_{ik} A_{ik}}, \qquad (1)$$

where A_{ij} and A_{ik} are the rates for transitions between the ith $1s^{-2}$ initial states and the jth $1s^{-1}2p^{-1}$ ($K^h\alpha$ transitions) or kth $2s^{-1}2p^{-1}$ final states ($K\alpha\alpha^h$ transitions), respectively. As shown in Table II, OIE (shake) processes that change the electronic configuration of deexcited K-shell hollow atoms, modify their radiative transition rates. In order to take into account this effect on the branching ratio, we used the equation

$$BR = \frac{I_0(K^h\alpha) + \sum_s I_s(K^h\alpha)\frac{I_s}{I_0}}{I_0(K\alpha\alpha^h) + \sum_s I_s(K\alpha\alpha^h)\frac{I_s}{I_0}}, \qquad (2)$$

where I_s/I_0 is the ratio of the intensity of the "diagram" $K^h\alpha$ and $K\alpha\alpha^h$ line (i.e., without additional spectator $3s$ or $3p$ vacancies), I_0, to the intensity of the its nl-shell satellite, I_s^{nl}.

The total shake probabilities, i.e., shake-off and shake-up, have been calculated by applying the sudden approximation model [42] and using MCDF wave functions for two valence ionization scenarios, namely, OIE1 and OIE2. The OIE1 corresponds to the ionization and/or excitation of the valence ($3s$ and $3p$) electrons due to the sudden atomic potential change resulting from the single K-shell vacancy. In the case of

TABLE III. Total shake probabilities (in percent per subshell) as a result of single (OIE1) and double (OIE2) K-shell ionization.

Subshell	Mg	Al		Si	
	3s	3s	3p	3s	3p
OIE1	20.62	11.81	15.08	7.89	18.24
OIE2	49.21	33.65	37.09	24.71	44.62

the OIE2, the more pronounced potential change is caused by two K-shell vacancies due to the quasisimultaneous removal of two $1s$ electrons (for details, see [12]). The calculated values of the total shake probabilities (in percent per subshell) for the OIE1 and OIE2 scenarios presented in Table III were used for the I_s/I_0 factor calculations in Eq. (2), employing the binomial distribution [43].

In Table IV the branching ratios for Mg, Al, and Si, calculated using various approaches, including OIE1 and OIE2, are presented and compared to the experimental data. One can see that employing the RCI and OIE1 approach improves distinctly the branching ratios over the simple MCDF model. The branching ratio values calculated by using the RCI+OIE2 model with the length gauge reproduces the measured branching ratios better than any other theoretical predictions published so far. Our calculations are also compared with the experimental values and previous theoretical predictions in Fig. 2. One can see that the inclusion of the $3s$ and $3p$ OIE2 contribution to the branching ratios reduces the discrepancies between the experiment and theory. The improvement is achieved at a relatively low cost related to the increase of differences between the length and velocity gauge branching ratio calculations within the RCI+OIE2 model by up to 6%. This is a natural consequence of taking into account the satellite TEOP transitions between states having in general more open subshells than those for the "diagram" ones. Nevertheless, only this approach can provide an atomic model that is able to take into account the OIE processes that can strongly affect TEOP transitions (see Table III).

In the next step of our studies, we made an attempt to reproduce the effective linewidth of the TEOP ($K\alpha\alpha^h$) transitions. The $K\alpha\alpha^h$ linewidth can be considered as the sum of the initial and the final atomic level widths:

$$\Gamma_{K\alpha\alpha^h} = \Gamma_{KK} + \Gamma_{L_1L_{2,3}}. \qquad (3)$$

TABLE IV. The $K^h\alpha$ to $K\alpha\alpha^h$ branching ratios for Mg, Al, and Si, calculated by using various approaches.

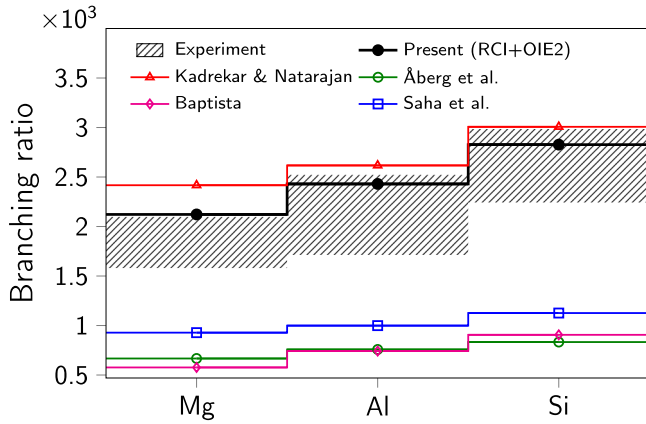|		Mg	Al	Si
MCDF	len	909	1002	1105
	vel	3102	3409	3807
RCI	len	2276	2644	3096
	vel	2363	2646	3148
RCI+OIE1	len	2200	2533	2964
	vel	2284	2605	3076
RCI+OIE2	len	2122	2418	2827
	vel	2205	2562	2998
Experiment: Ref. [3]		1838 ± 258	2115 ± 403	2610 ± 370

FIG. 2. Comparison between theoretical end experimental branching ratios for Mg, Al, and Si. Experiment: Hoszowska *et al.* [3]; theory: Åberg *et al.* [26], Baptista [25], Saha *et al.* [27], "Kadrekar & Natarajan" means compilation of data from Ref. [10] and Ref. [44].

So far, the widths of the KK and $L_1 L_{2,3}$ levels have been approximated by the expressions

$$\Gamma_{KK} \simeq 2\Gamma_K, \tag{4a}$$

$$\Gamma_{L_1 L_{2,3}} \simeq \Gamma_{L_1} + \Gamma_{L_{2,3}}. \tag{4b}$$

As was shown in Ref. [3], the theoretical predictions of TEOP linewidths based on Eqs. (4a) and (4b) underestimate the experimental values. In order to reliably reproduce the experimental values, one has to employ the fully relativistic calculations of the KK and $L_1 L_{2,3}$ level widths for double ionized states.

In our calculations of the KK level width we have summed the partial radiative $K^h \alpha_{1,2}$ (KK-$KL_{2,3}$) and $K^h \beta_{1,3}$ (KK-$KM_{2,3}$) and nonradiative KK-KLL and KK-KLM Auger widths, respectively. For the $L_1 L_{2,3}$ level width we have considered deexcitations of the $2s^{-1} 2p^{-1}$ state by the following channels: (a) by filling the L_1-shell hole by radiative L_1-$L_{2,3}$ and L_1-$M_{2,3}$ transitions or by filling the $L_{2,3}$-shell hole by radiative $L_{2,3}$-M_1 transitions (these transitions have lesser intensities); and (b) by nonradiative LL-LLM and LL-LMM Auger transitions. Calculations of nonradiative transition rates have been carried out by means of the FAC v1.1.4 [46] code, based on a modified Dirac-Hartree-Slater method. It has been found that taking into account the correlation effect by increasing the RCI expansion does not substantially change the Auger transition rates (the reduction was 0.7%–2.5% in the tested cases).

Our theoretical predictions for the widths of the KK and $L_1 L_{2,3}$ atomic levels, as well as the fluorescence yields (ω_{KK}) and the lifetime of the K^{-2} states (τ_{KK}), for Mg, Al, and Si, are collected in Table V. One can see in Table V that the KK and $L_1 L_{2,3}$ level widths obtained from the fully relativistic calculations are significantly larger (by up to a factor of ~ 2) than the approximation based on the sum of the single hole states [Eqs. (4a) and (4b)]. The newly improved theoretical values of the KK and $L_1 L_{2,3}$ level widths significantly reduce the discrepancy between the experimental and theoretical values of the $K \alpha \alpha^h$ linewidths [see column "Eq. (3)" in Table V]. In order to further improve the predictions of the
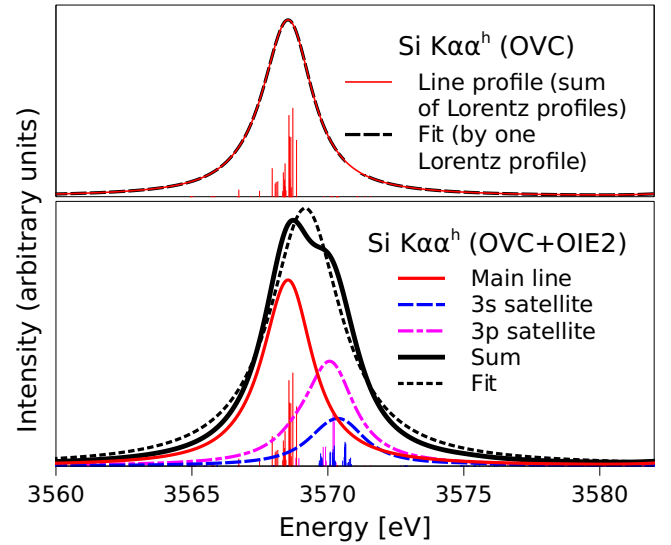

FIG. 3. The "diagram" and OIE2-originating satellite contributions to the width of the $K \alpha \alpha^h$ line of Si.

$K \alpha \alpha^h$ linewidth, it is necessary to extend the calculations to open-shell valence configuration (OVC) and OIE effects. The OVC effect is related to the open-shell atoms that have many initial and final states that can additionally broaden x-ray lines. The OVC broadening is a result of an overlap of many component x-ray lines having slightly different energies and widths. It has been previously shown that the OVC effect can enlarge the $K^h \alpha$ linewidths of atoms with $20 \leqslant Z \leqslant 30$ [12]. Details concerning the evaluation procedure for effective linewidths relating to the OVC effect can be found in Ref. [47].

Another reason for the broadening observed experimentally for the x-ray lines can be attributed to the OIE effect [12,47]. Ionization and excitation processes following the K-shell DPI lead to a larger contribution of the open-shell configurations amongst the deexciting atoms and, in consequence, to a broadening of the line. The evaluation procedure of the OIE effect (OIE2 scenario) is illustrated for Si in Fig. 3. It is worth noticing that the OIE effect affects not only the total TEOP linewidths but also the widths of the initial (KK) and final ($L_1 L_{2,3}$) levels. For example, the 3s and 3p OIE causes a reduction of the $L_1 L_{2,3}$ atomic level by up to 40%–60% (OIE2) because of the suppression of the LL-LLM and LL-LMM deexcitation channels. In columns "OIE1" and "OIE2" of Table V, the total TEOP linewidths are presented for the OIE1 and OIE2 ionization scenarios, respectively. As can be seen, only the theoretical predictions assuming strong shake processes (OIE2 scenarios) can reproduce all the experimental TEOP linewidths. This finding is consistent with our results obtained for branching ratios and with results in the previous studies [12] concerning $K^h \alpha_{1,2}$ hypersatellite linewidths. In the case of Mg and Al, the final elucidation of the OVC and OIE contributions to TEOP linewidths requires the measurements with a higher accuracy. Such results should ultimately verify the dominant role of the knockout character of DPI in the region of the K-shell DPI cross-section maxima that, in contrast to the pure shake-off mechanism, can initiate strong OIE processes (for details, see [3,12]).

TABLE V. Theoretical predictions for widths of KK and $L_1L_{2,3}$ atomic levels and $K\alpha\alpha^h$ linewidths.

Atom		Width of atomic level (eV)					τ_{KK}	Natural linewidths (eV)				
(conf. val.)		Γ_{KK}[a]	Eq. (4a) [45]	$\Gamma_{L_1L_{2,3}}$[a]	Eq. (4b) [45]	ω_{KK}	(10^{-16} s)	Eq. (3)	OVC	OIE1[b]	OIE2[b]	Expt. [3]
Mg	$3s^2$	0.901	0.66	1.032	0.49	0.0366	7.31	1.93	1.93	2.20	2.71	2.5 ± 0.6
Al	$3s^23p^1$	0.998	0.74	1.184	0.82	0.0491	6.60	2.18	2.31	2.68	3.06	2.9 ± 1.7
Si	$3s^23p^2$	1.094	0.86	1.342	0.95	0.0622	6.02	2.44	2.57	2.87	3.19	3.8 ± 0.9

[a]Average value per KK or $L_1L_{2,3}$ atomic level.
[b]Including influence of OIE1/OIE2 effect on the width of $L_1L_{2,3}$ atomic level.

In conclusion, we have shown that employing the MCDF-RCI calculations with OVC and OIE corrections enables one to reproduce the experimental TEOP linewidths and corresponding branching ratios for Mg, Al, and Si. The obtained theoretical values are in agreement within 7%–18% and 10%–14%

of the measured linewidths and branching ratios, respectively. Thus, the results of our studies set theoretical limits for the TEOP transitions in the low-Z atomic range. We also hope that this work will guide future theoretical studies for higher-Z elements and new experiments with a higher accuracy.

[1] E. P. Kanter, I. Ahmad, R. W. Dunford, D. S. Gemmell, B. Krässig, S. H. Southworth, and L. Young, Phys. Rev. A **73**, 022708 (2006).

[2] S. Huotari, K. Hämäläinen, R. Diamant, R. Sharon, C. C. Kao, and M. Deutsch, Phys. Rev. Lett. **101**, 043001 (2008).

[3] J. Hoszowska, J.-Cl. Dousse, J. Szlachetko, Y. Kayser, W. Cao, P. Jagodziński, M. Kavčič, and S. H. Nowak, Phys. Rev. Lett. **107**, 053001 (2011).

[4] L. Young, E. P. Kanter, B. Krässig, Y. Li, A. M. March, S. T. Pratt, R. Santra, S. H. Southworth, N. Rohringer, L. F. DiMauro, G. Doumy, C. A. Roedig, N. Berrah, L. Fang, M. Hoener, P. H. Bucksbaum, J. P. Cryan, S. Ghimire, J. M. Glownia, D. A. Reis, J. D. Bozek, C. Bostedt, and M. Messerschmidt, Nature (London) **466**, 56 (2010).

[5] L. J. Frasinski, V. Zhaunerchyk, M. Mucke, R. J. Squibb, M. Siano, J. H. D. Eland, P. Linusson, P. v.d. Meulen, P. Salén, R. D. Thomas, M. Larsson, L. Foucar, J. Ullrich, K. Motomura, S. Mondal, K. Ueda, T. Osipov, L. Fang, B. F. Murphy, N. Berrah, C. Bostedt, J. D. Bozek, S. Schorb, M. Messerschmidt, J. M. Glownia, J. P. Cryan, R. N. Coffee, O. Takahashi, S. Wada, M. N. Piancastelli, R. Richter, K. C. Prince, and R. Feifel, Phys. Rev. Lett. **111**, 073002 (2013).

[6] J. Arthur *et al.*, Linac Coherent Light Source (LCLS) Conceptual Design Report No. SLAC-R-593, SLAC, 2002, http://www-ssrl.slac.stanford.edu/lcls/cdr/.

[7] M. Altarelli *et al.*, XFEL: The European X-ray Free-Electron Laser Technical Design Report, Technical Report No. DESY 2006-097, DESY, 2006, http://xfel.desy.de/technical_information/tdr/tdr/.

[8] R. Diamant, S. Huotari, K. Hämäläinen, C. C. Kao, and M. Deutsch, Phys. Rev. A **62**, 052519 (2000).

[9] J. Rzadkiewicz, D. Chmielewska, T. Ludziejewski, P. Rymuza, Z. Sujkowski, D. Castella, D. Corminboeuf, J.-Cl. Dousse, B. Galley, Ch. Herren, J. Hoszowska, J. Kern, M. Polasik, and M. Pajek, Phys. Lett. A **264**, 186 (1999).

[10] R. Kadrekar and L. Natarajan, J. Phys. B **43**, 155001 (2010).

[11] J. Rzadkiewicz, D. Chmielewska, Z. Sujkowski, M. Berset, J.-Cl. Dousse, Y.-P. Maillard, O. Mauron, P.-A. Raboud, M. Polasik, K. Słabkowska, J. Hoszowska, and M. Pajek, Nucl. Instrum. Methods Phys. Res., Sect. B **235**, 110 (2005).

[12] M. Polasik, K. Słabkowska, J. Rzadkiewicz, K. Kozioł, J. Starosta, E. Wiatrowska-Kozioł, J.-Cl. Dousse, and J. Hoszowska, Phys. Rev. Lett. **107**, 073001 (2011).

[13] J. Hoszowska and J.-Cl. Dousse, J. Electron Spectrosc. Relat. Phenom. **188**, 62 (2013).

[14] W. Heisenberg, Z. Phys. **32**, 841 (1925).

[15] S. Goudsmit and L. Gropper, Phys. Rev. **38**, 225 (1931).

[16] W. Wölfli, C. Stoller, G. Bonani, M. Suter, and M. Stöckli, Phys. Rev. Lett. **35**, 656 (1975).

[17] A. R. Knudson, K. W. Hill, P. G. Burkhalter, and D. J. Nagel, Phys. Rev. Lett. **37**, 679 (1976).

[18] Ch. Stoller, W. Wölfli, G. Bonani, M. Stöckli, and M. Suter, Phys. Rev. A **15**, 990 (1977).

[19] R. Schuch, G. Gaukler, and H. Schmidt-Böcking, Z. Phys. A **290**, 19 (1979).

[20] J. Volpp, R. Schuch, G. Nolte, and H. Schmidt-Böcking, J. Phys. B **12**, L325 (1979).

[21] H. Tawara and P. Richard, Can. J. Phys. **80**, 1579 (2002).

[22] S. I. Salem, A. Kumar, B. L. Scott, and R. D. Ayers, Phys. Rev. Lett. **49**, 1240 (1982).

[23] M. S. A. L. Al-Ghazi, J. Birchall, and J. S. C. McKee, Phys. Rev. A **25**, 3072 (1982).

[24] Y. Isozumi, Phys. Rev. A **22**, 1948 (1980).

[25] G. B. Baptista, J. Phys. B **17**, 2177 (1984).

[26] T. Åberg, K. A. Jamison, and P. Richard, Phys. Rev. Lett. **37**, 63 (1976).

[27] J. Saha, T. K. Mukherjee, S. Fritzsche, and P. K. Mukherjee, Phys. Lett. A **373**, 252 (2009).

[28] J. Hoszowska, J.-Cl. Dousse, W. Cao, K. Fennane, Y. Kayser, M. Szlachetko, J. Szlachetko, and M. Kavčič, Phys. Rev. A **82**, 063408 (2010).

[29] P. Jönsson, G. Gaigalas, J. Bieroń, C. F. Fischer, and I. P. Grant, Comput. Phys. Commun. **184**, 2197 (2013).

[30] K. G. Dyall, I. P. Grant, C. Johnson, F. A. Parpia, and E. Plummer, Comput. Phys. Commun. **55**, 425 (1989).

[31] I. P. Grant, *Relativistic Quantum Theory of Atoms and Molecules*, Springer Series on Atomic, Optical, and Plasma Physics Vol. 40 (Springer, New York, 2007).

[32] B. J. McKenzie, I. P. Grant, and P. H. Norrington, Comput. Phys. Commun. **21**, 233 (1980).

[33] P. J. Mohr and Y.-K. Kim, Phys. Rev. A **45**, 2727 (1992).

[34] L. W. Fullerton and G. A. Rinker, Jr., Phys. Rev. A **13**, 1283 (1976).

[35] I. P. Grant, J. Phys. B **7**, 1458 (1974).

[36] F. A. Babushkin, Acta. Phys. Pol. **25**, 749 (1964).

[37] C. F. Fischer, M. Godefroid, T. Brage, P. Jönsson, and G. Gaigalas, J. Phys. B **49**, 182004 (2016).

[38] C. T. Chantler, A. C. L. Hayward, and I. P. Grant, Phys. Rev. Lett. **103**, 123002 (2009).

[39] C. T. Chantler, J. A. Lowe, and I. P. Grant, Phys. Rev. A **82**, 052505 (2010).

[40] A. M. Costa, M. C. Martins, J. P. Santos, P. Indelicato, and F. Parente, J. Phys. B **39**, 2355 (2006).

[41] C. F. Fischer, T. Brage, and P. Jönsson, *Computational Atomic Structure: An MCHF Approach* (IOP Publishing, Bristol, 1997).

[42] T. A. Carlson, C. W. Nestor, Jr., T. C. Tucker, and F. B. Malik, Phys. Rev. **169**, 27 (1968).

[43] J. H. McGuire and P. Richard, Phys. Rev. A **8**, 1374 (1973).

[44] L. Natarajan, Phys. Rev. A **78**, 052505 (2008).

[45] J. L. Campbell and T. Papp, At. Data Nucl. Data Tables **77**, 1 (2001).

[46] M. F. Gu, Can. J. Phys. **86**, 675 (2008).

[47] K. Kozioł, J. Quant. Spectrosc. Radiat. Transfer **149**, 138 (2014).